



# Thermally induced optical nonlinearity in colloidal alloy nanoparticles synthesized by laser ablation

M. Abdullah<sup>1</sup> · H. Bakhtiar<sup>2,3</sup> · M. S. A. Aziz<sup>2,3</sup> · G. Krishnan<sup>2,3</sup> · N. A. M. Ropi<sup>4</sup> · N. Kasim<sup>1</sup> · N. N. Adnan<sup>4</sup>

Received: 7 August 2018 / Accepted: 23 July 2019 / Published online: 1 August 2019  
© Springer-Verlag GmbH Germany, part of Springer Nature 2019

## Abstract

Colloidal suspension of alloy nanoparticles has been prepared and their third-order nonlinear optical response was investigated by means of the Z-scan technique, employing 532 nm continuous wave laser excitation. Alloys colloidal suspension of industrial grade brass, aluminium, and copper was prepared via laser ablation in liquid technique. FESEM analysis reveals the particles size of less than 102.33 nm on average. The magnitude and sign of the nonlinear refraction,  $n_2$  and nonlinear absorption,  $\beta$  were determined. It was observed from the closed aperture Z-scan that all the suspensions exhibited a self-focusing effect with a negative nonlinear refractive index,  $n_2$ , attributed to thermal lensing effect. Colloids of brass possess highest  $n_2$  followed by copper and aluminium suspension, attributed to the thermally agitated process whereby heat is transferred into non-local region of the propagation axis. Open Z-scan results revealed that the brass suspension exhibited saturable absorption (SA) with significant negative  $\beta$  value. Aluminium and copper alloy NPs suspension rather shows reverse saturable absorption with a positive  $\beta$  value. These materials were found to exhibit significant nonlinear refraction and nonlinear absorption behaviour, making them possible candidates for photonic and/or optoelectronic applications, especially with low powered continuous wave laser excitation.

## 1 Introduction

Metal nanoparticles (NPs) have attracted great interest in recent years because of their distinct optical properties and their advances in various applications such as sensors, bio-medical, and optoelectronics devices [1]. Most commonly gold, silver and copper NPs and its alloys have been studied extensively [2]. Composite/bimetallic NPs, especially, have gained special significance due to their unique tunable optical properties [3]. Linear and nonlinear optical properties

of composite NPs such as Au/Ag coreshells [3, 4], CdS NPs [5], Au/Pd NPs [6], Cu/SiO nanocomposite [7], PbS NPs [8], Cu/Au mixture NPs [9], and Mn/ZnO films [10] have been reported previously [11].

Better understanding on the contribution of optical properties can be achieved by studying different metal NPs [12]. These materials are easiest to be synthesised via laser ablation in liquid medium technique (LASIS) to form a colloidal NPs suspension [13]. Gold and silver are the common targets that have been extensively studied using this technique but, up to our knowledge, alloys made of brass, copper and aluminium have never been reported. The same technique has been successful in synthesis of binary alloy NPs from its bulk alloy as the target, such as CoPt [14], PtAu [15, 16], NiFe and SmCo [17], AgAu [18], and AuFe [19]. In our project, we ablated three different kinds of alloys that are commonly used: brass, aluminium alloys, and copper to produce colloidal NPs suspension.

The tightly focused laser beam can easily induce the temperature change in the colloidal system. The thermal conductivity of a colloid measures the rate of temperature change in a transient heat transfer process. Therefore, owing to heat transfer processes in the thermo-optical effects, they can be very important in the thermal nonlinear response of

✉ M. Abdullah  
mundzirabdullah@yahoo.com

<sup>1</sup> Institute of Nano Optoelectronics Research and Technology (INOR), Universiti Sains Malaysia (USM), 11800 Gelugor, Penang, Malaysia

<sup>2</sup> Laser Center, Ibnu Sina for Scientific and Industrial Research, Universiti Teknologi Malaysia, Johor Bahru, Johor, Malaysia

<sup>3</sup> Department of Physics, Faculty of Sciences, Universiti Teknologi Malaysia, 81310 Johor Bahru, Johor, Malaysia

<sup>4</sup> Department of Science, Faculty of Science, Technology and Human Development, Universiti Tun Hussein Onn, Batu Pahat, Johor, Malaysia

a nanostructure system. Sarkhoush et al. reported that higher nonlinear refractive index value of Au colloids was reported at higher thermal conductivity colloids [2]. Since brass, copper, and aluminium alloys have different thermal conductivity, the control of temperature gradient rate is an important factor for producing high thermal nonlinear properties in materials. In this study, we have studied the nonlinear optical properties of alloys NPs via single-beam Z-scan setup using continuous wave 532 nm laser excitation.

## 2 Materials and methods

### 2.1 Preparation of alloys NPs

Industrial grade of brass, aluminium, and copper sample in the form of plate were used as the target in LASiS process. EDX analysis reveals the elemental analysis on each alloys. The thermal conductivity of the alloys and the solvent has been taken from the literature and is listed in Table 1 [20].

Laser ablation of the alloy samples was performed using fundamental wavelength of Nd:YAG laser in distilled water. Approximately, 800 pulses of 1064 nm at the energy of 125 mJ were used for ablation. Figure 1a illustrates the ablation process and the image of targets and suspensions is shown in Fig. 1b. Water has very low nonlinearity and

thermal conductivity, so the solvent effect towards the nonlinear behaviour in the colloids can be neglected.

### 2.2 Linear optical properties

The linear absorption coefficient,  $\alpha$ , at 532 nm was calculated based on the absorbance value and tabulated in Table 2. The refractive index,  $n$ , of the alloy suspensions was measured using a digital refractometer (DR201-95, KRUSS).

### 2.3 Nonlinear optical characterization

The laser used is a continuous wave diode pumped solid state (DPSS) laser (Coherent Verdi-V5, 532 nm). The detector used is silicon amplified photodetector (PDA55, Thorlabs). The suspension was contained in a quartz cuvette with a pathlength of 1 mm which was mounted onto a precision motorized stage (LTS-300, Thorlabs). The sample pathlength is much smaller than the Rayleigh length at 0.94 cm, which is an essential prerequisite for Z-scan thin sample analysis. During the scan, the cuvette was moved along the Z-direction of the laser beam under the control of a computer. A 50:50 beam splitter was used to split the beam into two arms. One of the two photodetectors used was placed after an aperture for the first arm (closed Z-scan), while the other was placed in front of a lens for the second arm (open Z-scan). Concurrently, the signal from the two photodetectors was monitored and recorded by an oscilloscope. The phenomena that contribute to nonlinear refraction will be studied from closed

**Table 1** Thermal conductivity of alloys targets

Suspension	Thermal conductivity (W/mK)
Brass	14–109
Cu alloy	46–237
Al alloy	112–205
Water	0.591

**Table 2** Linear absorption coefficient of the alloy suspensions

Suspension	$\alpha$ (cm <sup>-1</sup> )
Brass	-0.74772
Aluminium	-0.57139
Copper	-0.40622

**Fig. 1** a NPs synthesis via LASiS, b brass, aluminium, and copper alloy (from left, top) and its colloidal suspension (bottom)

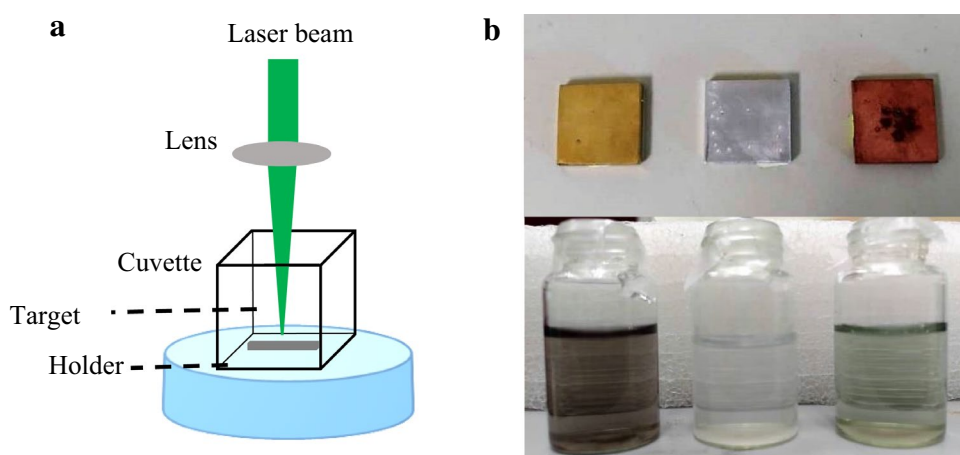


**Table 3** Z-scan parameters

Parameters	Value
$f$	20 cm
$r_a$	0.068 cm
$w_0$	0.0023 cm
$\lambda$	532 nm
$S$	0.22
$z_r$	0.94 cm

aperture Z-scan, while the open aperture Z-scan will be sensitive towards the nonlinear absorption response. Table 3 summarizes the parameters of the Z-scan setup used in the experiment.

The peak followed by a valley-normalized transmittance obtained from the closed aperture Z-scan is defined as  $\Delta T_{p-v}$  which is given as  $T_p - T_v$ . The variation of this quantity as a function of  $|\Delta\phi_0|$  is given by  $\Delta T_{p-v} = 0.406(1 - S)^{0.25} |\Delta\phi_0|$ , where  $|\Delta\phi_0|$  is the on-axis phase shift at the focus;  $S$  is the aperture linear transmittance with  $r_0$  denoting the aperture radius ( $S = 1 - \exp(-2r_0^2/\omega_0^2)$ ), and  $\omega_0$  denoting the beam radius at the aperture in the linear regime. Then, the nonlinear refractive index,  $n_2$ , is given by

$$n_2 = \frac{\Delta\phi_0 \lambda}{2\pi I_0 L_{\text{eff}}}, \quad (1)$$

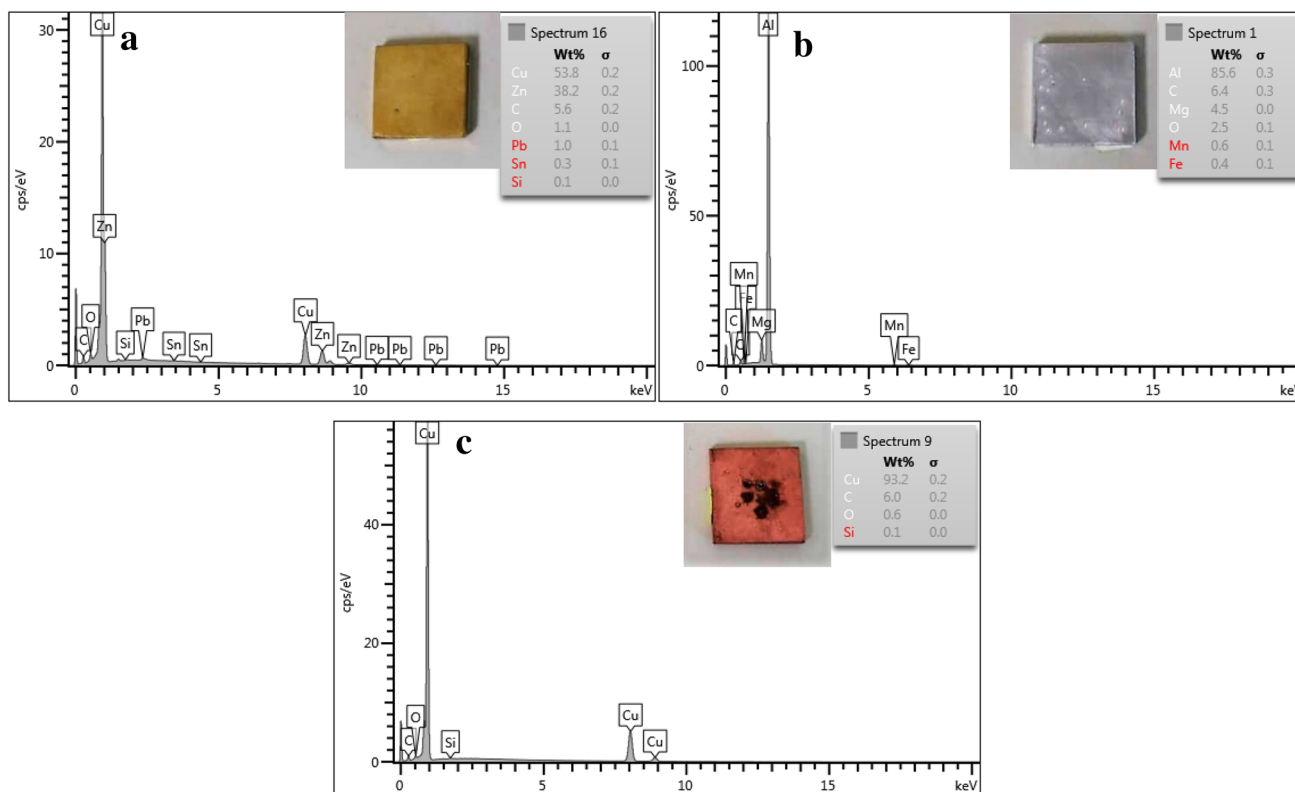
where  $\lambda$  is the laser wavelength,  $I_0$  is the intensity of the laser beam at focus  $z = 0$ ,  $L_{\text{eff}} = \frac{[1 - \exp(-\alpha L)]}{\alpha}$ ,  $L_{\text{eff}}$  is the effective thickness of the sample,  $\alpha$  is the linear absorption coefficient and  $L$  is the thickness of the sample. The nonlinear absorption coefficient,  $\beta$ , can be estimated from the open aperture Z-scan data. The normalized transmittance for the open aperture condition is given by

$$T(z, s = 1) = \sum_{m=0}^{\infty} \frac{[-q_0(z)]^m}{(m+1)^{3/2}}, \quad (2)$$

or  $q_0(z) < 1$ , where  $q_0(z) = \frac{\beta I_0 L_{\text{eff}}}{(1 + z^2/z_R^2)}$ ,  $z_R = k\omega_0^2/2$  is the diffraction length of the beam and  $\omega_0$  is the beam waist radius at the focal point and  $k = 2\pi/\lambda$  is the wave vector.

## 2.4 Characterization of the alloy nanoparticles

The nanoparticles have been characterized using field emission scanning electron microscope (FESEM) coupled

**Fig. 2** EDX spectra of the target and its images of the alloy targets (inset)

with energy dispersive X-ray (EDX) and dynamic light scattering (DLS).

### 3 Results and discussion

EDX spectra in Fig. 2 indicated the elemental composition of the alloy targets used during the LASiS process. Brass alloys contained mostly Cu and Zn, with slight traces of carbon C, Pb, Sn and Si. Aluminium target is majorly composed of Al–Mg alloy, and slight percentage of Mn and Fe, while copper target contained 93% of Cu with negligible

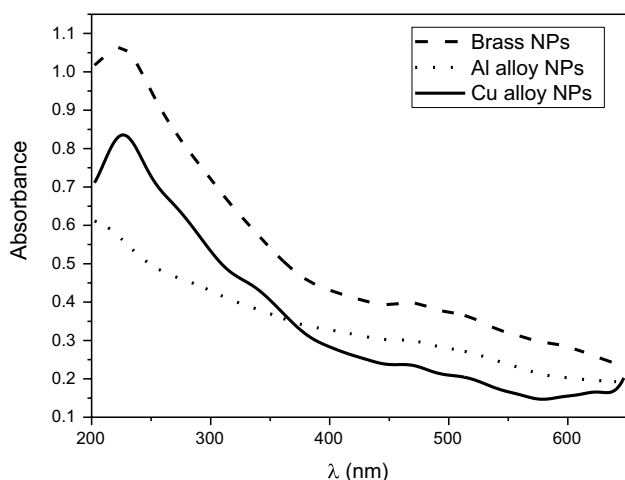


Fig. 3 UV–Vis spectra of the alloy NPs suspensions

impurities. Figure 3 shows the UV–Vis absorption spectra of the three colloidal suspension, brass, aluminium and copper alloys. All samples showed no absorption band in the visible regime. The absorption at the Z-scan laser excitation (532 nm) was recorded, from which the linear absorption coefficient,  $\alpha$ , was calculated. Overall, the brass colloids have higher absorbance within the visible region as compared to aluminium and copper colloids which explains the darker colour of the suspension as in Fig. 2.

The brass NPs were characterized using FESEM, EDX, and DLS as shown in Fig. 4a–c, respectively. FESEM micrograph shows the generated brass NPs with an average size of 17.94 nm. Some particles appear to accumulate and form a bigger particle. EDX point analysis confirms the alloy form of the NPs with Cu and Zn as the main element presents, as well as small percentage of Sn, Pb, Al and Mn. The size distribution from DLS, however, shows trimodal distribution which suggests the non-uniformity of the NPs. This is the result of the agglomeration of the particles during and after the ablation process. The first mode of the DLS was the contribution of the non-agglomerated nanoparticles (peak ~ 20 nm), while the middle mode where the intensity is highest represents the agglomerated particles up to the size of ~ 100 nm. The presence of larger particles in DLS graph (3rd peak in Fig. 4c) comes from the presence of droplets spatters and sideways spatters during intense ablation process.

FESEM micrograph of the Al alloys NPs in Fig. 5a shows larger particles with an average size of 102.33 nm. The large-sized spatters can be clearly seen in Fig. 5a. The

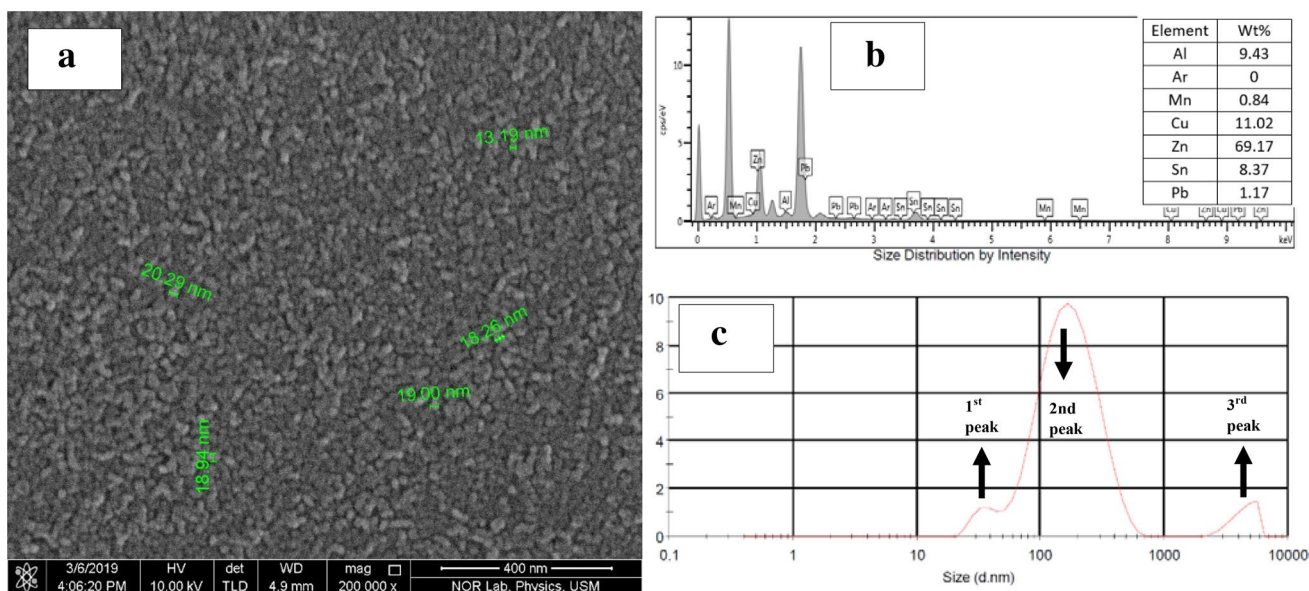


Fig. 4 Characterization of brass suspension for Z-scan measurement. **a** FESEM image of the nanoparticles, **b** EDX spectra of particles, and **c** particle size distribution from DLS



presence of Al, Mg and Na in the EDX spectrum confirmed the alloyed structure of the particles. The DLS analysis in Fig. 5c failed to analyse the size distribution of particles as it mostly contained large pieces from the spatters and the agglomerated particles. The agglomeration is more prominent in Al NPs because of its lower melting temperature (463–671 °C); thus, the agglomeration occurs during

subsequent laser pulses as the melting process starts to occur. The result is the formation of instantaneous molten Al alloy within the solvent. Subsequently, particles with nonuniform size distribution were produced during LASiS process of Al alloys as the target.

Figure 6a shows the FESEM image of the Cu NPs. The average particle size is 30.96 nm with EDX analysis

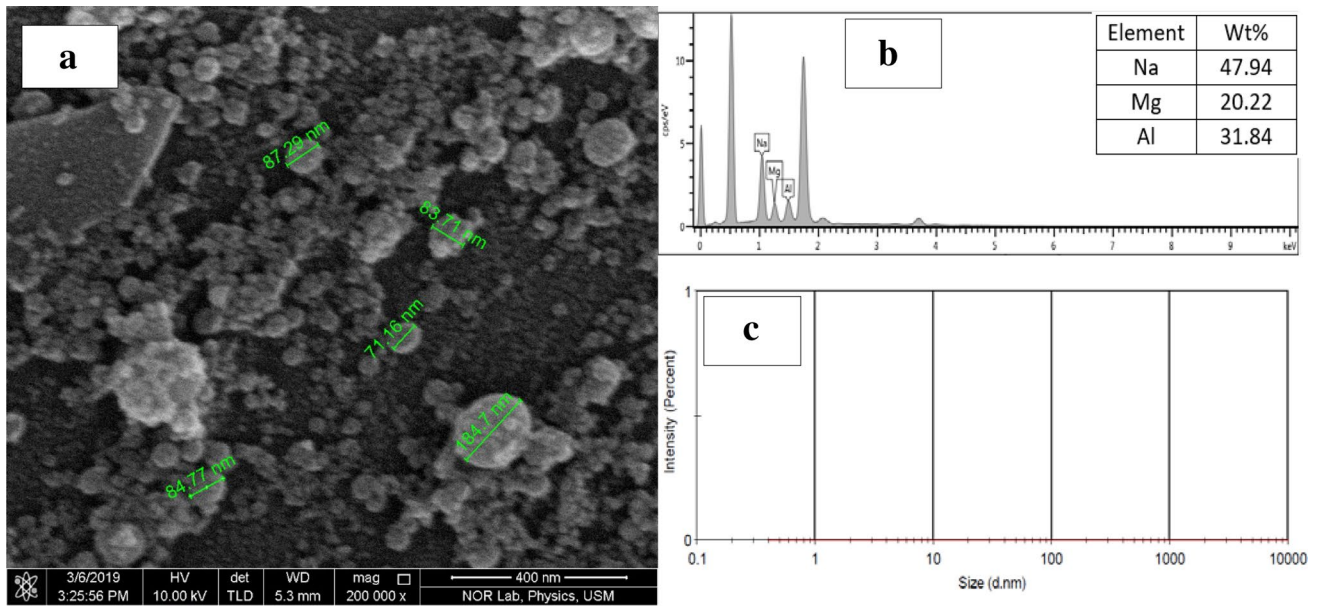


**Fig. 5** Characterization of aluminium suspension for Z-scan measurement. **a** FESEM image of the nanoparticles, **b** EDX spectra of particles, and **c** particle size distribution from DLS

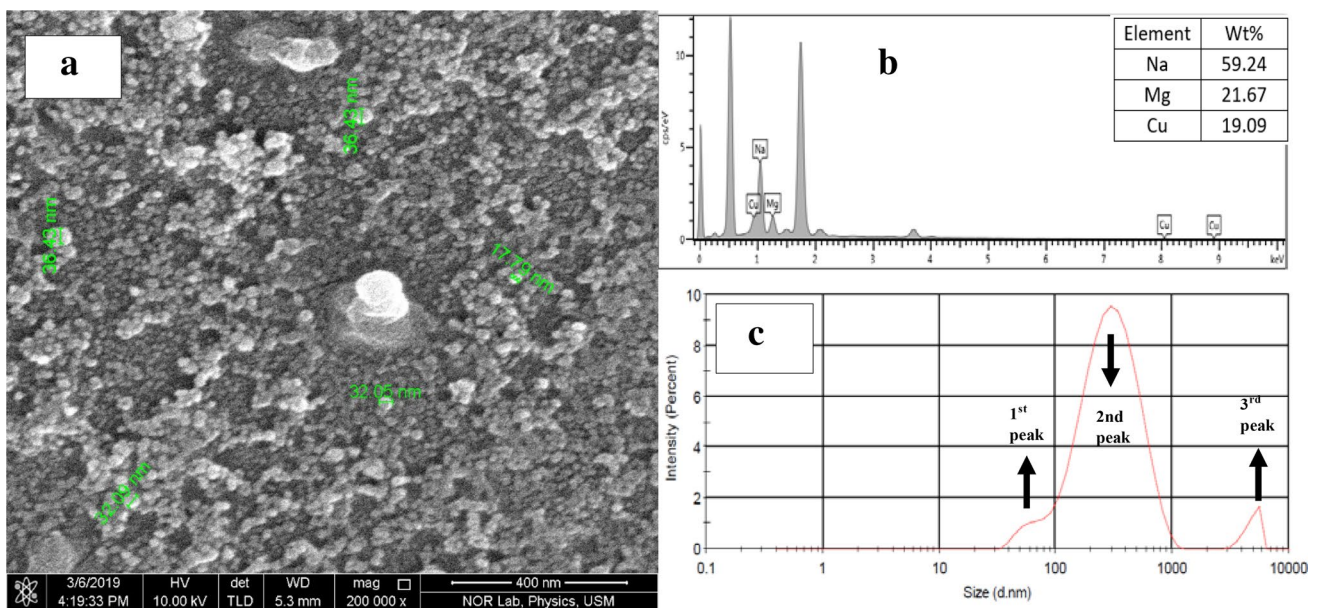


**Fig. 6** Characterization of Cu NPs for Z-scan measurement. **a** FESEM image of the nanoparticles, **b** EDX spectra of particles, and **c** particle size distribution from DLS

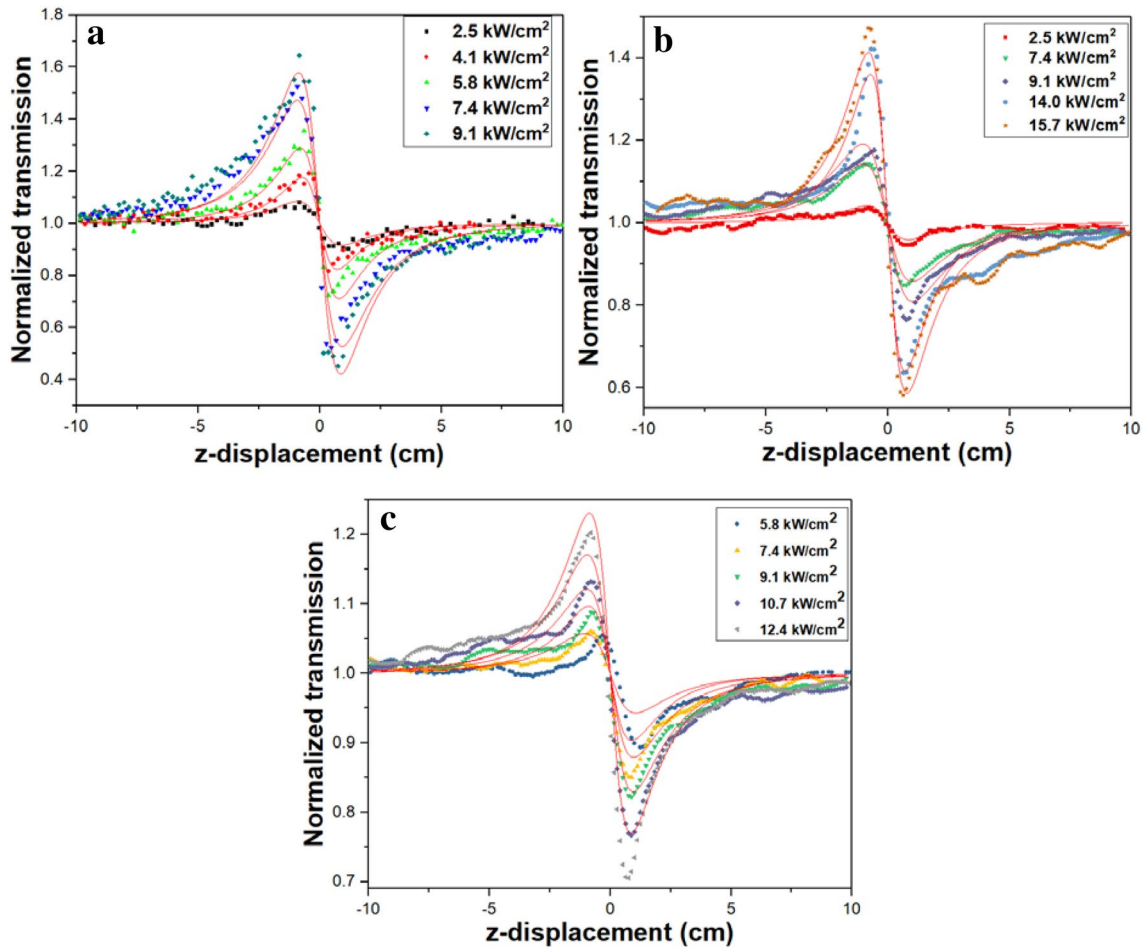


**Fig. 7** Closed-aperture Z-scan results for the **a** brass, **b** Al alloy and **c** Cu alloys NPs suspensions

revealing alloys with the content of Cu, Mg and Na. The size distribution from DLS showing trimodal distribution peaked at  $\sim 40$  nm,  $\sim 150$  nm, and  $\sim 4000$  nm. The 1st peak is the contribution from each individual particle as shown in Fig. 6a and the 2nd peak represents the agglomerated particles with size (in diameter) up to 1000 nm, while the last peak speaks for the spatters formation as discussed before.

The original concentration of the colloid suspensions after the ablation was maintained during Z-scan experiments without dilution. The output signal from closed Z-scan for the samples is plotted in Fig. 7. The solid line represents the theoretical fit to the experimental data all showing good correlation with the data. With an aperture of size 0.68 mm placed in the far field of the samples, the resulting transmittance exhibited a self-defocusing effect with a symmetrical peak–valley curve. The physical origin of nonlinear refraction can be electronic, molecular, electrostrictive or thermal in nature. In the present case, the nonlinearity is thermal in nature as CW laser was used as the excitation source. The agitated thermal effect will increase the excited state

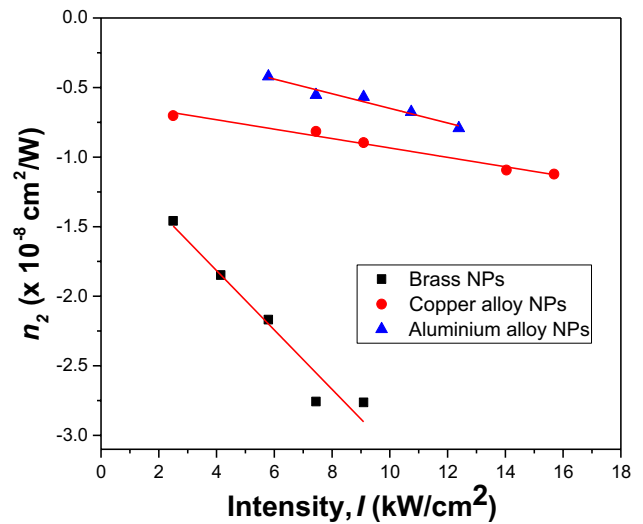


**Fig. 8** The dependency of  $n_2$  towards the intensity for each suspension

absorption (ESA). The  $z$  separation between the peak and valley was calculated to be  $> 1.7z_r$ , which clearly indicates thermal nonlinearity (for ideal Gaussian beam for third-order nonlinearity,  $z = 1.7z_r$ ) [21, 22]. Quantitative analysis on the nonlinear refraction behaviour of the samples reveals a negative nonlinear refractive index,  $n_2$ . The value of  $n_2$  is plotted against the focal intensity in Fig. 8.

As the suspension passes through the tightly focused beam, part of the energy is absorbed by the metal NPs and converted into heat. This results in change of the refraction index of the suspension and the path of the laser beam creating what is known as thermal lensing. At higher laser excitation energy, higher local temperature is induced. Ideally, for pure third-order nonlinearity the value of  $n_2$  should be independent of the intensity. However, it is interesting to note in Fig. 8 that the value of  $n_2$  is dependent on the

intensity, which indicates the contribution from thermally induced nonlinearity. Thus, the nonlinearity observed is temperature dependent and this contributes to a stronger nonlinearity of the samples. The thermal conductivity of water as the solvent is much lower compared to the thermal conductivity of the particles; therefore, we can assume that the thermal diffusion that occurs within the beam waist occurs through conduction during collision between the nanoparticles. By comparison, the value of  $n_2$  in the increasing order is brass NPs, Cu alloy NPs, and Al alloy NPs. This order can be explained due to the contribution of the particle size, as smaller particle size (higher mobility, more collisions) tends to dissipate heat quicker into the beam spot area and, consequently, results in severe phase distortion of the propagating beam (Fig. 9).

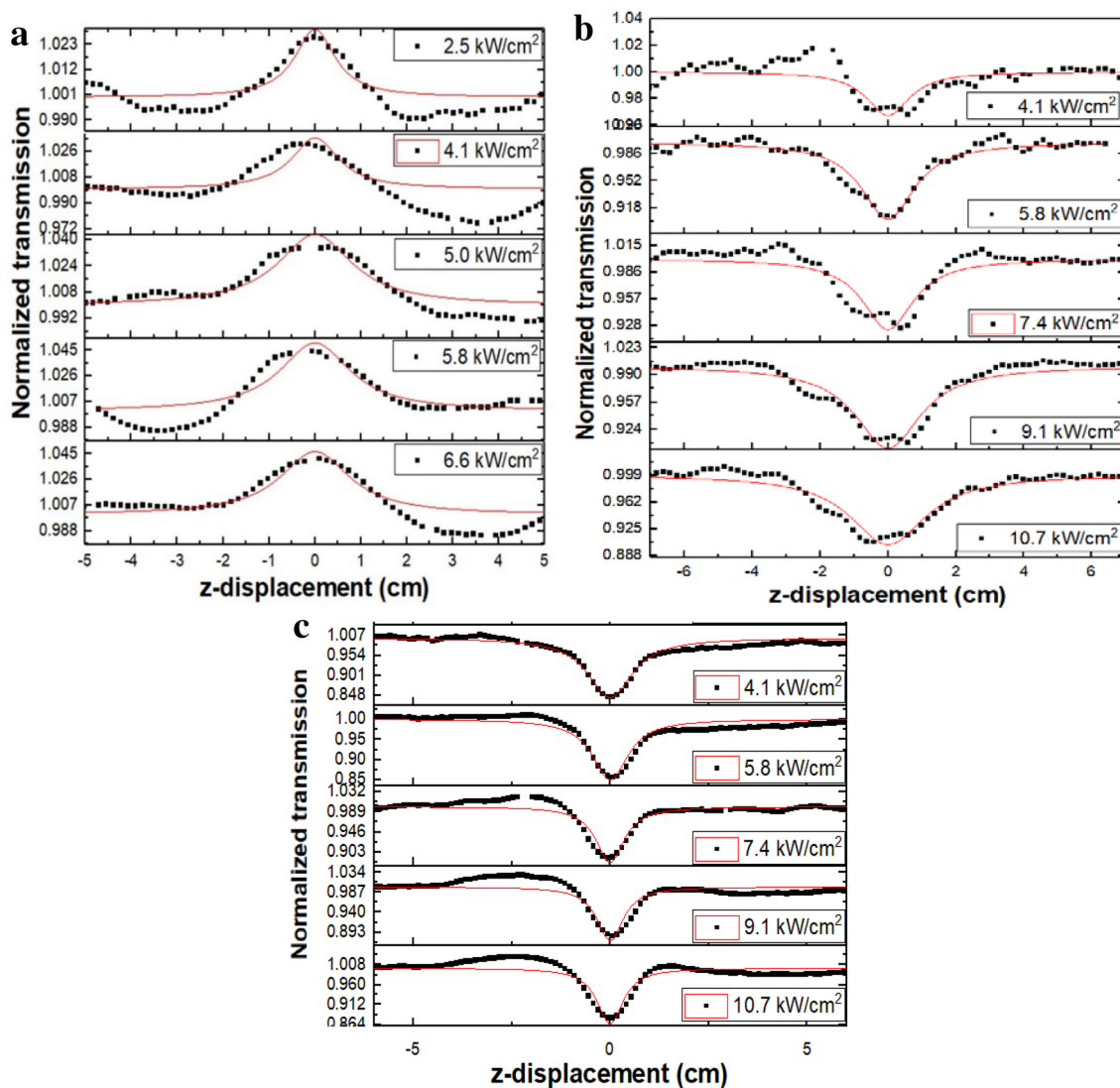


**Fig. 9** Open aperture Z-scan signal of the **a** brass, **b** Al alloys, and **c** Cu alloys NPs suspensions

The open Z-scan curves of the suspensions are shown in Fig. 5. Interestingly, brass NPs exhibited strong saturable absorption (SA) within the laser intensity tested. This is caused by the depletion of electrons in ground state, i.e. ground state bleaching. At the tightly focused beam, the electrons in the ground state of the brass NPs are excited into an upper energy state at a rate that is faster than their subsequent relaxation back to the ground state. The same behaviour has been reported for other metallic NPs such as platinum NPs [23], silver NPs in glass [24] and gold NPs [4]. Figure 10 shows that the value of  $\beta$  for the brass NPs decreases in value with increasing focal intensity which illustrates that the optical bleaching effect is reduced at higher intensity. Thus, the results obtained in this work demonstrate that brass NPs suspension could be used as saturable absorber for mode-locked lasers, especially for low intensity laser.

On the contrary, Al alloy NPs and Cu alloy NPs showed reverse saturable absorption (RSA) phenomena within the intensity range of 4.1–10.7 kW/cm<sup>2</sup>. Surface plasmon resonance (SPR) for Al and Cu NPs occurs below 250 nm (Fig. 2), far from the excitation wavelength of 532 nm used, which implies that the SPR mechanism is not contributing to the nonlinear absorption. RSA can be caused by several nonlinear optical processes including two photons absorption (2PA), excited state absorption, nonlinear scattering and free carrier absorption. The magnitude of  $\beta$  was calculated via nonlinear curve fitting according to Eq. 2 by Levenberg–Marquardt algorithm. Our results showed that Cu suspension possesses highest positive  $\beta$  value while highest negative  $\beta$  value was recorded for brass suspension. It is worth noting that the magnitude of the  $n_2$  and  $\beta$  of these

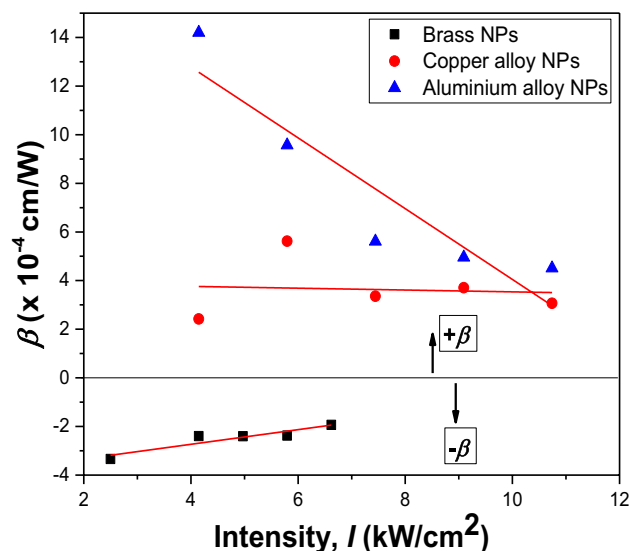


**Fig. 10** The dependency of  $\beta$  towards the focal intensity for each suspension

alloys suspensions is comparable with some of the common studied metal NPs such as gold and silver [25]. Therefore, these materials have the potential to be exploited in the developing various photonics and optoelectronics devices.

## 4 Conclusions

We have reported the nonlinear optical response of brass, copper and aluminium alloys nanoparticles in colloidal forms. The FESEM analysis reveals the nanoparticles sized 19.94 nm for brass NPs, 102.33 nm on average. The colloids were synthesised by laser ablation in liquid medium technique. All suspensions exhibited a self-focusing effect with a negative nonlinear refractive index,  $n_2$ , attributed to thermal lensing effect. The brass nanoparticle exhibited SA properties, while the aluminium and copper alloys exhibited reverse saturable absorption at higher intensity.

**Acknowledgements** The authors would like to thank the Malaysia Ministry of Education and Universiti Teknologi Malaysia for their financial support through Tier 1 with vote 18H67. Special thanks also to Universiti Teknologi Malaysia for the postdoctoral scheme under vote number 04E08 for the first author.

## References

1. A.R. Sadrolhosseini, A.S.M. Noor, N. Faraji, A. Kharazmi, M.A. Mahdi, *J. Nanomater.* **2014**, 962917 (2014)
2. L. Sarkhosh, N. Mansour, *Laser Phys.* **25**, 65404 (2015)
3. E. Kirubha, P.K. Palanisamy, *Adv. Nat. Sci. Nanosci. Nanotechnol.* **5**, 045006 (2014)
4. J.T. Seo, Q. Yang, W.-J. Kim, J. Heo, S.-M. Ma, J. Austin, W.S. Yun, S.S. Jung, S.W. Han, B. Tabibi, D. Temple, *Opt. Lett.* **34**, 307 (2009)
5. N. Venkatram, D.N. Rao, M.A. Akundi, *Opt. Express* **13**, 867 (2005)
6. J.L.J. Pérez, R. Gutiérrez-Fuentes, J.F.S. Ramírez, O.U.G. Vidal, D.E. Téllez-Sánchez, Z.N.C. Pacheco, A.C. Orea, J.A.F. García, *Adv. Nanoparticles* **02**, 223 (2013)
7. Y.H. Wang, Y.M. Wang, J.D. Lu, L.L. Ji, R.G. Zang, R.W. Wang, *Opt. Commun.* **283**, 486 (2010)
8. H.P.P. Li, B. Liu, C.H.H. Kam, Y.L.L. Lam, W.X.X. Que, L.M.M. Gan, C.H.H. Chew, G.Q.Q. Xu, *Opt. Mater. (Amst.)* **14**, 321 (2000)
9. Y.H. Wang, Y.M. Wang, C.J. Han, J.D. Lu, L.L. Ji, R.W. Wang, *Phys. B Condens. Matter* **405**, 2848 (2010)
10. K.K. Nagaraja, S. Pramodini, A. Santhosh Kumar, H.S. Nagaraja, P. Poornesh, D. Kekuda, *Opt. Mater. (Amst.)* **35**, 431 (2013)
11. Y.X. Zhang, Y.H. Wang, *RSC Adv.* **7**, 45129 (2017)
12. O. Sánchez-Dena, O. Baldovino-Pantaleón, S. Almaguer-Valenzuela, J.A. Reyes-Esqueda, E.V. García-Ramírez, *Opt. Express* **24**, A154 (2015)
13. V. Amendola, M. Meneghetti, *Phys. Chem. Chem. Phys.* **11**, 3805 (2009)
14. T. Seto, K. Koga, H. Akinaga, F. Takano, T. Orii, M. Hirasawa, *J. Nanoparticle Res.* **8**, 371 (2006)



15. J. Zhang, G. Chen, D. Guay, M. Chaker, D. Ma, *Nanoscale* **6**, 2125 (2014)
16. J. Zhang, D.N. Oko, S. Garbarino, R. Imbeault, M. Chaker, A.C. Tavares, D. Guay, D. Ma, *J. Phys. Chem. C* **116**, 13413 (2012)
17. J. Jakobi, S. Petersen, A. Menéndez-Manjón, P. Wagener, S. Barcikowski, *Langmuir* **26**, 6892 (2010)
18. A. Neumeister, J. Jakobi, C. Rehbock, J. Moysig, S. Barcikowski, *Phys. Chem. Chem. Phys.* **16**, 23671 (2014)
19. S. Scaramuzza, S. Agnoli, V. Amendola, *Phys. Chem. Chem. Phys.* **17**, 28076 (2015)
20. F. Cverna, *ASM Ready Reference: Thermal Properties of Metals*, 1st edn. (ASM International, Ohio, 2002)
21. V. Viswanath, S.S. Nair, G. Subodh, C.I. Muneera, *SN Appl. Sci.* **1**, 43 (2019)
22. S.J. Mathews, S.C. Kumar, L. Giribabu, S.V. Rao, *Mater. Lett.* **61**, 4426 (2007)
23. Y. Gao, X. Zhang, Y. Li, H. Liu, Y. Wang, Q. Chang, W. Jiao, Y. Song, *Opt. Commun.* **251**, 429 (2005)
24. A. Ajami, W. Husinsky, B. Svecova, S. Vytykacova, P. Nekvindova, *J. Non. Cryst. Solids* **426**, 159 (2015)
25. T. Jia, T. He, P. Li, Y. Mo, Y. Cui, *Opt. Laser Technol.* **40**, 936–940 (2008)

**Publisher's Note** Springer Nature remains neutral with regard to jurisdictional claims in published maps and institutional affiliations.